# Evaluation of fiber radius mapping using diffusion MRI under clinical system constraints

**C-H. Yeh[1,2], I. Kezele[1], D. Alexander[3], B. Schmitt[1], J-R. Li[1], D. Le Bihan[1], C-P. Lin[2], and C. Poupon[1]**

[1]NeuroSpin, I2BM, CEA, Gif-sur-Yvette, France, [2]National Yang-Ming University, Taipei, Taiwan, [3]University College London, London, United Kingdom

## Introduction

The advanced diffusion-weighted (DW) MR microscopy imaging is a useful tool to probe microstructural features of tissues, such as cell size, fiber density, and membrane permeability [1-3]. These direct measures of tissue properties can be utilized as biomarkers to monitor tissue status. Although a number of elaborate imaging protocols have been proposed for microstructures imaging [4-5], the conventional pulsed-gradient spin-echo (PGSE) sequence remains the most commonly used especially on clinical MR scanners due to the constraints on the gradient system. The method described in [1] is able to effectively optimize the DW MR imaging protocol for measuring the fiber/cellular sizes found in the human brains, whereas the difficulties for clinical studies remain in two aspects. Firstly, the optimized imaging strategy is generated for a specific fiber radius, whereas the white matter (WM) of human brain covers a range of fiber diameter approximately from 1 to 10 μm; secondly, a high gradient intensity (at least 70 mT/m) is required for accurate estimation of small fiber radius, which is less feasible to clinical MR scanners where the maximum gradient amplitude is limited to 40 mT/m. Accordingly, in this study, we used a Monte Carlo simulator to simulate water diffusion in various fiber radii, and then evaluate a list of PGSE imaging protocols under the constraint on the gradient system capability of clinical MR scanners.

## Methods

Simulations were performed using a random walk Monte Carlo simulator to simulate 3D water molecular diffusion in a bundle of parallel impermeable fibers formed by mesh-based cylinders [6]. We created four simulation scenes with the same the intracellular fraction ($f_{IC}$=0.74), where each contains specific fiber radius $R$(=1/2/4/6 μm). In each simulation scene, $10^5$ diffusing particles were randomly distributed, and a constant diffusivity of $2\times10^{-3}$ mm$^2$/s was assumed to be identical in the intra- and extra-cellular space. We used a total iteration count of $10^4$ and a simulation time step of 10 μs, yielding a step size of 0.32 μm.

Synthetic MR dataset was obtained by simulating a PGSE sequence with trapezoidal DW gradient pulses [6]. Table 1 summarized the list of imaging protocols created to conform to the capability of clinical MR system. Each protocol contains 120 DW acquisitions with different $M$ and $N$ combinations, where $M$ is the number of $q$-space sampling shells and $N$ is the number of DW gradient orientations per shell. In each protocol, the gradient amplitude and slew rate were fixed at 40 mT/m and 200 T/m/s respectively, while the DW gradient pulse duration (δ) and separation (Δ) were varied simultaneously to keep a constant effective diffusion time ($\Delta_{eff}=\Delta-\delta/3=50$ ms) so as to reach sufficient diffusion sensitizing factors (i.e. $b$-values) for short δs. Note that all of the $b$-values used in this study were all clinically achievable. The echo time (TE) determined by the maximum δ and Δ was fixed in each protocol, and a T2 of 70 ms typically found in WM at 3T was used.

Parameter estimation was performed using the Markov Chain Monte Carlo (MCMC) method implemented with a Rician noise model to sample the posterior distribution of model parameters [1-2]. Initial estimates for $f_{IC}$, axial and transverse diffusivities were obtained from the diffusion tensor analysis on the synthetic dataset. Fiber direction (along z-axis) and radius ($R$) were initialized to the ground-truth values given in the Monte Carlo simulations. Synthetic Rician noise was added to the DW signal considering the effect of varying TE between the protocols. The signal-to-noise ratio was 50 on the null DW signal at TE=86.5 ms. In the procedure of MCMC, the burn-in period, sampling interval, and sampling count were $10^5$, $10^3$, and $10^2$ respectively. The MCMC was repeated for 10 times to collect $10^3$ samples.

## Results & Discussion

Fig. 1 shows the histograms of $R$ estimates obtained from the posterior distribution for each true radius $R$, and Table 2 summarizes the mean and standard deviation ($\sigma$) of the distributions for each case. All of the protocols accurately estimated large radii ($R$=4 and 6 μm) but produced bias for small radii, especially for $R$=1 μm; nevertheless, it could be still recognized as a small size. For $M$=3 (i.e. *Protocol 1-3*), *Protocol 3* resulted in better $R$ estimation than the others, indicating that moderate to high $b$-values were important for accurate $R$ mapping. The similar findings were observed when $M$=4 and 5: *Protocol 6&8* utilized higher $b$-values and resulted in sharper distributions, i.e. lower $\sigma$. *Protocol 3* ($M$=3), *6* ($M$=4), and *8* ($M$=5) resulted in less overlapping between $R$=1 and 2 μm, and produced sharper distribution for larger radii. Furthermore, *Protocol 3* was better in terms of accuracy and precision, which implied that introducing low $b$-value shells might spread distribution.

## Conclusion

We assessed the feasibility in mapping fiber radii under the constraints of clinical MR systems. Within clinical acceptable acquisition time (~30 minutes), we observed that using three shells with moderate to high $b$-values (*Protocol 3*) is potentially feasible to estimate fiber/cellular sizes with minimum overlapping between distributions. Further work will consider more realistic biological conditions, such as the effect of size distribution, permeability, angular dispersion of the fibers.

## References

[1] Alexander DC. MRM 2008; 60:439-448. [2] Alexander DC *et al*. NeuroImage 2010; 52:1374-1389. [3] Assaf Y *et al*. MRM 2008; 59:1347-1354. [4] Shemesh N *et al.* JMR 2009; 198:15-23. [5] Xu J *et al.* JMR 2009; 200:189-197. [6] Yeh CH *et al.* Proc ISMRM 2010; 2241.

**Table 1. Clinical PGSE DW MR imaging protocols**

| *Protocol* | M | N | δ (ms) | TE (ms) | *b*-value (s/mm$^2$) |
|---|---|---|---|---|---|
| 1 | 3 | 40 | 4, 8, 12 | 70.5 | 80, 350, 800 |
| 2 | | | 8, 16, 20 | 81.2 | 350, 1430, 2250 |
| 3 | | | 16, 20, 24 | 86.5 | 1430, 2250, 3250 |
| 4 | 4 | 30 | 4, 8, 12, 16 | 75.8 | 80, 350, 800, 1430 |
| 5 | | | 8, 12, 16, 20 | 81.2 | 350, 800, 1430, 2250 |
| 6 | | | 12, 16, 20, 24 | 86.5 | 800, 1430, 2250, 3250 |
| 7 | 5 | 24 | 4, 8, 12,16, 20 | 81.2 | 80, 350, 800, 1430, 2250 |
| 8 | | | 8, 12,16, 20, 24 | 86.5 | 350, 800, 1430, 2250, 3250 |
| 9 | 6 | 20 | 4, 8, 12,16, 20, 24 | 86.5 | 80, 350, 800, 1430, 2250, 3250 |

**Table 2. Mean ± Standard deviations ($\sigma$) of the distributions**

| *Protocol* | *R*=1 μm | *R*=2 μm | *R*=4 μm | *R*=6 μm |
|---|---|---|---|---|
| 1 | 1.54 ± 0.68 | 2.11 ± 0.61 | 4.11 ± 0.68 | 5.70 ± 0.65 |
| 2 | 1.22 ± 0.44 | 1.78 ± 0.33 | 3.91 ± 0.29 | 6.07 ± 0.58 |
| **3** | 1.02 ± 0.31 | 1.86 ± 0.26 | 3.88 ± 0.33 | 5.91 ± 0.34 |
| 4 | 1.07 ± 0.50 | 1.93 ± 0.65 | 3.81 ± 0.50 | 6.11 ± 0.41 |
| 5 | 1.17 ± 0.31 | 1.84 ± 0.53 | 3.93 ± 0.48 | 6.11 ± 0.54 |
| *6* | 1.04 ± 0.27 | 1.78 ± 0.30 | 3.90 ± 0.38 | 6.12 ± 0.44 |
| 7 | 1.29 ± 0.35 | 1.95 ± 0.63 | 3.92 ± 0.44 | 6.22 ± 0.43 |
| *8* | 0.96 ± 0.32 | 1.79 ± 0.26 | 3.92 ± 0.27 | 5.94 ± 0.41 |
| 9 | 1.14 ± 0.37 | 1.69 ± 0.47 | 3.91± 0.35 | 6.00 ± 0.37 |

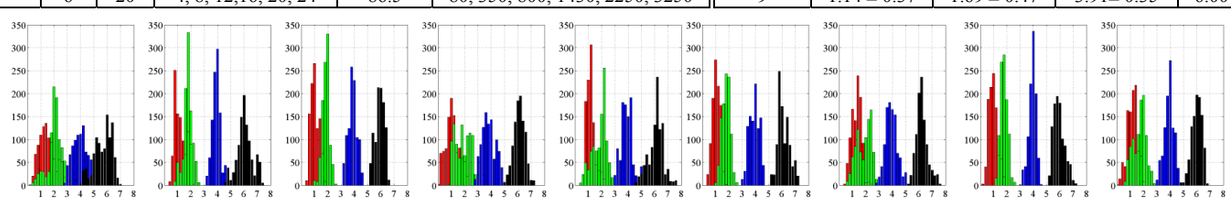

**Fig. 1**: Histograms of samples obtained from the MCMC posterior distributions on $R$ (red/green/blue/black: $R$=1/2/4/6 μm). Left to right: *Protocol 1* to *Protocol 9*.